ADVANCED FUNCTIONAL MATERIALS
www.afm-journal.de

Chemical Interface Structures in CdS/RbInSe$_2$/Cu(In,Ga)Se$_2$ Thin-Film Solar Cell Stacks

*Jakob Bombsch, Tim Kodalle, Raul Garcia-Diez, Claudia Hartmann, Roberto Félix, Shigenori Ueda, Regan G. Wilks, Christian A. Kaufmann, and Marcus Bär**

Performance-enhancing heavy alkali-based post-deposition treatments (PDT) of Cu(In,Ga)Se$_2$ (CIGSe) thin-film solar cells absorbers often induce the formation of a Rb- In-Se phase on the CIGSe absorber. Co-evaporation of an interfacial RbInSe$_2$ (RISe) layer between buffer and absorber can also benefit cell performance. A detailed analysis of the chemical interface structures in CdS/RISe/CIGSe layer stacks is performed using hard X-ray photoelectron spectroscopy (HAXPES). For comparison, stacks without RISe and based on RbF PDT CIGSe absorbers are also studied. When aiming for the direct co-evaporation of a RISe layer on the CIGSe absorber, the formation of an additional In-Se phase is found. For the RbF PDT CIGSe absorbers, the study only finds small amounts of Rb and no indication for a RISe layer formation. Examining layer stacks prepared via additional chemical bath deposition (CBD) of CdS reveals a clear impact of the presence of Rb (or of Rb-containing species) on the CIGSe surface. In these cases, an increase of the induction/coalescence period is found at the beginning of the CBD buffer layer growth process and the formation of Cd—Se bonds; thereafter, a more compact CdS layer growth is observed.

1. Introduction

The implementation of post deposition treatments (PDTs) based on heavy alkali metal fluorides into the deposition process of Cu(In,Ga)Se$_2$ (CIGSe) absorber layers has led to significant increases in device efficiency of resulting solar cells over the recent years.[1–3] One of the reported effects of such PDTs is the formation of an alkali-In-Se phase, which was predicted for the alkali metals K, Rb, and Cs[4] and has been observed in the cases of KF and RbF PDTs.[5–8] While the overall effect of optimized PDTs is positive, a too pronounced alkali-In-Se phase is frequently associated with an energetic barrier having a detrimental impact on the fill factor (*FF*) in the case of RbF PDT.[9,10] To examine the distinct impact of the Rb-In-Se (RISe) phase on the solar cell performance, Kodalle et al. replaced the RbF PDT by a direct RISe co-evaporation of varying duration.[9] Despite a detrimental impact on the *FF* for longer deposition times, an overall increase in device performance could be detected due to significant gains in open circuit voltage (V_{OC}).

To understand this efficiency increase, we used hard X-ray photoelectron spectroscopy (HAXPES) to perform a detailed analysis of the chemical structure of RISe/CIGSe heterostructures manufactured in the same way as in ref [9]. For comparison, an untreated

J. Bombsch, R. Garcia-Diez, C. Hartmann, R. Félix, R. G. Wilks, M. Bär
Department Interface Design
Helmholtz-Zentrum Berlin für Materialien und Energie GmbH (HZB)
12489 Berlin, Germany
E-mail: marcus.baer@helmholtz-berlin.de

T. Kodalle, C. A. Kaufmann
PVcomB
HZB
12489 Berlin, Germany

S. Ueda
Synchrotron X-ray Station at SPring-8
National Institute for Materials Science (NIMS)
1-1-1 Kouto, Sayo, Hyogo 679-5148, Japan

The ORCID identification number(s) for the author(s) of this article can be found under https://doi.org/10.1002/adfm.202403685

DOI: 10.1002/adfm.202403685

S. Ueda
Research Center for Electronic and Optical Materials
NIMS, 1-1 Namiki, Tsukuba, Ibaraki 305-0044, Japan

R. G. Wilks, M. Bär
Energy Materials In-Situ Laboratory Berlin (EMIL)
HZB
12489 Berlin, Germany

M. Bär
Department of X-ray Spectroscopy at Interfaces of Thin Films
Helmholtz-Institute Erlangen-Nürnberg for Renewable Energy (HI ERN)
12489 Berlin, Germany

M. Bär
Department of Chemistry and Pharmacy
Friedrich-Alexander-Universität Erlangen-Nürnberg (FAU)
91058 Erlangen, Germany

and a RbF PDT CIGSe absorber were also studied. In addition, we deposited a CdS thickness series on some of those samples to investigate the impact of the respectively altered surfaces on the buffer layer growth.

2. Results and Discussion

Survey spectra of the differently treated CIGSe absorbers and the RISe reference[11] are shown in Figure S1 (Supporting Information). They indicate the presence of all CIGSe related elements on all samples except for the RISe reference, where no signs of Cu and Ga are visible. In addition, oxygen- and carbon-related signals are observed, which might be attributed to surface contaminants, which were either not removed by the NH_4OH etching or adsorbed to the surface in the time between rinsing and measurement (e.g., when the samples were handled in ambient condition directly prior to HAXPES measurements). However, the inclusion of some O and C into the bulk of the absorber (during deposition) is also a possible scenario. In addition, the alkali elements Na and Rb are indicated to be present at all sample surfaces with two exceptions: The (control) untreated CIGSe absorber shows no indications for the presence of Rb, and the RbF PDT absorber surface does not exhibit any sign for the presence of an appreciable amount of Na, in agreement with previous findings of RbF PDT leading to Na free CIGSe surfaces.[12,13] For a thorough investigation of the chemical surface structure, detail-spectra of the related shallow core levels were obtained. The Rb 3d, Ga 3p, Cu 3p, and Na 2s spectra can all be fitted with one component for all samples (see Figure S2, Supporting Information), indicating that the presence of Rb on the RbF PDT CIGSe and RISe/CIGSe samples does not result in the formation of additional chemical environments for Ga, Cu, or Na.

However, the Se 3d and In 4d related peaks undergo significant changes induced by the RISe evaporation which needs to be accounted for by the introduction of additional contributions in the fit model. It is possible to model the changes in line shape of these spectra by curve fit analysis using only one additional spectral contribution; however, such a model leads to significant inconsistencies as discussed extensively in the Supporting Information in conjunction with Figures S3 and S4 (Supporting Information). To reach meaningful data interpretations fits employing two additional spectral contributions are needed, as presented in **Figure 1**, where the Se 3d and Ga 3d/In 4d spectra of the different samples are displayed alongside with that of the RISe reference. The "a" fit component of the Se 3d and In 4d spectra is attributed to CIGSe throughout, with observable shifts between samples attributable to changes in electronic structure as a result of differing surface treatments. The "a" component and the "d" component of the In 4d spectra, attributed to oxidized In (as regularly observed on CIGSe[6,14]) are the only spectral contributions for the untreated and RbF PDT absorber data. Additional "b" and "c" contributions are required to properly fit the spectra of the RISe/CIGSe sample set. The position of the "b" contribution, which is shifted to lower BE, agrees with an assignment to a RISe phase for both Se and In.[6] This assignment is corroborated by the main species of the RISe reference appearing at similar positions and are labelled Se_b and In_b. The secondary "c" contribution appears at similar BE in the RISE reference and RISe/CIGSe sample measurements; appearing in both, Se 3d and In 4d, it might be related to an additional In-Se bond environment. [NB: the widths of the fit functions in the RISE reference spectra have a ≈0.1 eV higher Gaussian width than in the other spectra, and the separation between the "b" and "c" components differs. These changes may indicate that the origin of the peaks in the RISE reference differs in some way despite the close agreement.] This assumption is further corroborated by a previous Raman study on identically produced RISe reference samples, indicating the presence of one or more In–Se-type species besides the main RISe phase.[15] However, it is difficult to make any statements on the precise nature of the In–Se-type compound(s) and whether they are identical on the RISe reference and the RISe/CIGSe samples. The absolute BE positions of all different core levels and species are given in Table S1 (Supporting Information).

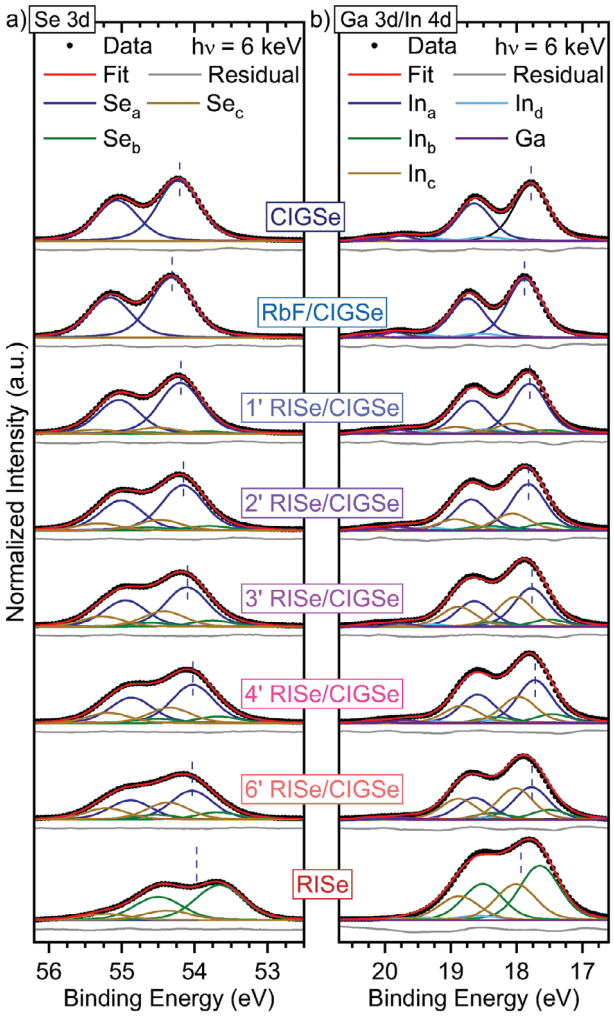

Figure 1. HAXPES (6 keV) spectra of RISe/CIGSe samples prepared using different RISe deposition times (resulting in different thicknesses) as well as of a RbF PDT absorber, a bare (untreated) CIGSe, and a RISe ref. [11] for comparison. a) Se 3d and b) Ga 3d/In 4d spectra are displayed. Data are shown with a linear background subtracted. Respective fits using pairs of Voigt profiles to represent the respective doublets are displayed along the data as well as the respective residuals. The vertical dashed lines mark the position of the "a" species as a visual guide; the separation between species was held constant in the fitting procedure.

In contrast to the clear changes of the chemical environment of Se and In of the RISe/CIGSe samples, no indications for the formation of additional species can be found for the RbF PDT CIGSe absorber, which is in contrast to previous studies, where the formation of a Rb-In-Se phase could be observed as a result of RbF PDT.[6,8] However, the relatively high nominal [Cu]/([In]+[Ga]) ratio (*CGI*) of 0.95 of the samples used in this study (compared to, e.g., 0.9 in ref. [8]) might reduce the amount of RISe phase formed to below the detection limit of our HAXPES measurements, which are also less surface sensitive than the conventional XPS measurements used in ref. [13].

The nominal thickness of the cover layer was calculated from the attenuation of the CIGSe absorber core level spectral signatures (Cu 3p, Ga 3p, Se_a 3d, and In_a 4d; Figure 1; Figure S2, Supporting Information) using the Lambert–Beer law and assuming homogeneous coverage and an IMFP of 8.6 nm (as would be expected for a RISe layer) as derived by QUASES IMFP TPP2M code.[16,17] The results, displayed in **Figure 2**a, indicate increasing cover layer thicknesses with increasing RISe deposition times, as expected. The RbF PDT (leftmost in Figure 2a) causes a small intensity decrease of the core level spectral intensity compared to the untreated absorber, consistent with an average cover layer thickness of (0.2 ± 0.2) nm, which is thinner than a monolayer of all suspected phases; therefore a non-closed layer is assumed, in agreement with the previously observed "nanopatterning" on similar absorbers.[13] The cover layer thicknesses estimated from the different photoemission lines are all in agreement, indicating the absence of significant diffusion of any absorber-related element toward the sample's surface as a result of RISe deposition. To corroborate this, the [Ga]/([Ga]+[In]) (*GGI*) and *CGI* ratios were calculated based on the total intensities of the given elements and considering only the CIGSe-related species (Cu, Ga, and In_a) and are displayed as red triangles in Figure 2b,c, respectively. The *GGI* and *CGI* considering only the CIGSe-related contributions remain constant within the error bars, showing that the absorber composition itself is unaffected by RISe deposition. When the calculated using total intensities (i.e., all In photoemission signal), the *GGI* and *CGI* decrease with increasing RISe deposition times, in agreement with the deposition of a Ga- and Cu-free cover layer.

The overall [Na]/([Cu]+[In]+[Ga]+[Se]) and [Rb]/([Cu]+[In]+[Ga]+[Se]) ratios were calculated as measures for the respective alkali content in the samples and are displayed in Figure 2d. While Na is completely removed from the surface region by the RbF PDT, in agreement with previous observations,[12,13] no such Na depletion is found after the RISe deposition. While the Na content slightly changes for the different RISe thicknesses/RISe deposition time, no clear trend can be found, indicating a different interaction mechanism between Rb and Na in case of the RISe deposition compared to the RbF PDT, which might positively impact the device efficiency as discussed in ref. [9].

While the RbF PDT leads to some Rb deposition on the sample surface, its amount is significantly less, even compared to the shortest RISe deposition time. The deposited Rb amount is also significantly smaller compared to that resulting from a combined NaF/RbF PDT on low temperature (LT) absorbers,[6] the value of which is presented as an open triangle in Figure 2d for comparison. This corroborates the comparable small quantitative impact

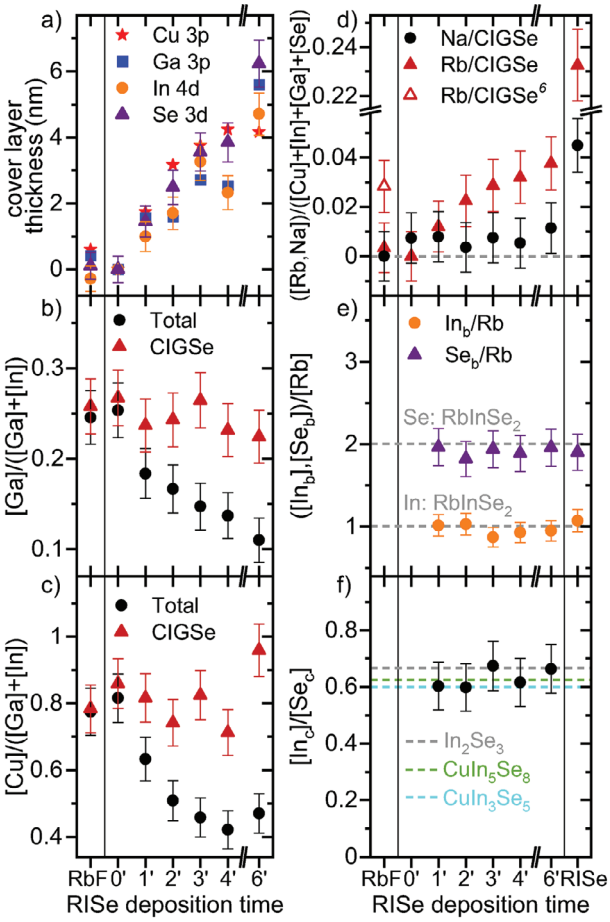

Figure 2. a) RISe layer thickness calculated on the basis of core level attenuation. Calculated thicknesses are given for each core level individually. b) Total [Ga]/([Ga]+[In]) ratio (GGI) and GGI calculated using only Ga and In_a species and therefore only referring to the GGI in the CIGSe phase. c) Total [Cu]/([Ga]+[In]) ratio (CGI) and CGI calculated using only Cu, Ga, and In_a species and therefore only referring to the CGI in the CIGSe phase. d) [Rb]/([Cu]+[In]+[Ga]+[Se]) and [Na]/([Cu]+[In]+[Ga]+[Se]) ratios as a measure of respective alkali content. For comparison, the [Rb]/([Cu]+[In]+[Ga]+[Se]) ratio of low-temperature CIGSe after RbF PDT from ref. [6] is given. e) $[In_b]/[Rb]$ and $[Se_b]/[Rb]$ ratios as a measure of stoichiometry in the additionally formed "b phase". The gray dashed lines indicate the respective positions for a stoichiometric $RbInSe_2$ compound. f) $[In_c]/[Se_c]$ ratio as an indication of the stoichiometry in the additional "c compound". The dashed lines indicate the expected composition for In_2Se_3, $CuIn_5Se_8$, and $CuIn_3Se_5$.

of the RbF PDT on the chemical structure of the CIGSe absorber (with nominal *CGI* = 0.95 and in particular on the chemical environment of Se and In) in this study, as already discussed above. The Rb content increases for increasing RISe deposition times, reaching a [Rb]/([Cu]+[In]+[Ga]+[Se]) ratio of ≈0.04 (±0.01) for 6 min. However, this is significantly less than expected for a stoichiometric RISe layer for the following reason: From the effective cover layer thicknesses (Figure 2a) and the decrease in total *GGI* and *CGI* (black circles, Figure 2b,c) we can conclude that, in the case of the 6 min RISe sample, about half of the signal originates from the absorber and half from the cover layer. However, the amount of Rb on the 6 min sample is less than 20% of what is

observed on the pure RIS sample, which itself seems to possess a Rb-depleted surface region ([Rb]/([Cu]+[In]+[Ga]+[Se]) ≈0.23, while the value for stoichiometric $RbInSe_2$ would be 0.33). Therefore, the amount of Rb is less than 40% of what would be expected in the stated scenario, indicating that the deposited cover layer is significantly Rb depleted compared to the RISe reference or stoichiometric $RbInSe_2$, even though the deposition conditions were nominally identical. As significant diffusion of CIGSe related elements into the cover layer can be excluded, as discussed above, this indicates that a significant fraction of the Rb diffuses out of the deposited layer during or after deposition. This assumption is also corroborated by the fact that glow-discharge optical emission spectrometry (GDOES) measurements on identically produced samples show significant amounts of Rb inside the bulk of the CIGSe absorber after a RISe evaporation also indicating a significant diffusion of Rb into the CIGSe.[9,18]

The observed Rb deficiency in RISe layers would be in agreement with different scenarios: A very Rb-deficient Rb–In–Se-type layer could be formed, similar to the Cu deficient vacancy compound frequently suggested to form on the CIGSe front surface.[6–8] However, it could also be, that an additional separate phase forms parallel to $RbInSe_2$, which would be in agreement with the additional Se_c and In_c species discussed above.

To investigate the stoichiometry of the RISe phase, the In_b/Rb and Se_b/Rb ratios were calculated and are plotted in Figure 2e. Both ratios agree within the error with a Rb:In:Se stoichiometry of 1:1:2 (i.e., with a proposed $RbInSe_2$[4]). To get a quantitative perspective on the In-Se related second species, the In_c/Se_c ratio was derived and is depicted in Figure 2f. While the determined ratios would be, e.g. in agreement with the formation of In_2Se_3, or a Cu:In:Se = 1:5:8 or 1:3:5 ordered vacancy compound, an unambiguous assignment would require further investigation. Note, also a mixture of different In-Se containing phases would be a reasonable explanation.

To elaborate how the different surfaces impact the CdS buffer layer growth, CdS layers of different thicknesses were deposited on the untreated and RbF PDT absorbers as well as on the 2 and 4 min RISe/CIGSe samples. Survey scans of the samples (Figure S5, Supporting Information) display the presence of Cd and S and attenuation of CIGSe related peaks after CdS deposition. Analysis of the Se 3s/S 2s, Cd 4s/Rb 3d/Ga 3p, Cu 3p, Se 3d, and Ga 3d/ In 4d detail spectra (Figures S6–S8, Supporting Information) indicates the presence of one S species, which is assigned to CdS, and two Cd species, of which the dominant species is also assigned to CdS, while a minor contribution at higher BE is attributed to oxidized Cd, probably related to the air exposure of the samples prior to measurement. No additional species are required to fit the chalcopyrite related core levels after the CdS deposition, however, in the case of the Se 3d peak, changes in the peak shape lead to a relative intensity change of the different Se contributions, further discussed below.

To get a better impression of the buffer layer growth dynamics, the attenuation of the Ga 3p, Cu 3p, Se 3d, and In 4d peaks (Figures S6 and S7, Supporting Information) was used to calculate the buffer layer thickness using the Lambert-Beer law and an IMFP of 9.8 nm assuming homogeneous CdS coverage (Figure S9, Supporting Information). The average values obtained from the different core levels are displayed in **Figure 3**a. When comparing the CdS layer thicknesses for the different

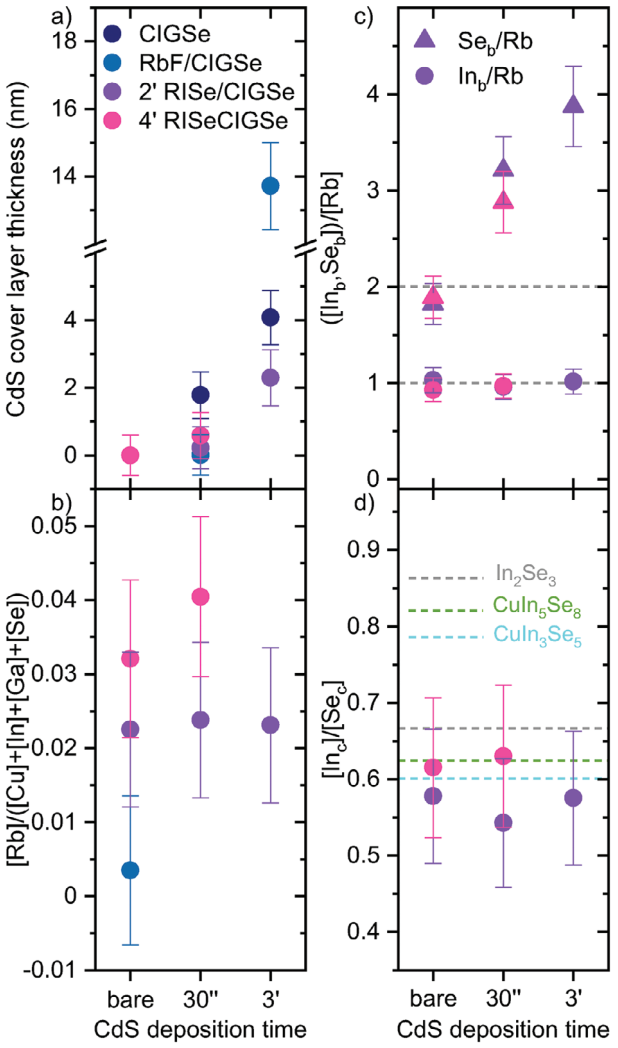

Figure 3. a) CdS layer thickness calculated as averages from individual core level attenuation (Figure S9, Supporting Information). b) [Rb]/([Cu]+[Ga]+[In]+[Se]) ratios as a measure of Rb content. c) $[In_b]/[R_b]$ and $[Se_b]/[R_b]$ ratios as a measure of stoichiometry in the additional formed "b phase" related to RISe. The grey dashed lines indicate the respective positions for a stoichiometric $RbInSe_2$ compound. d) $[In_c]/[Se_c]$ ratio as an indication of stoichiometry in the additional "c compound", consisting of In and Se. The dashed lines indicate the expected composition for In_2Se_3, $CuIn_5Se_8$, and $CuIn_3Se_5$.

(RISe/)CIGSe samples, substantial differences are found: While a 2 nm layer is formed on the untreated CIGSe layer already after 30 s, the derived layer thickness is close to zero after the same time on the RbF PDT CIGSe sample and the absorbers with RISe, indicating a delayed/slower growth of the buffer on the Rb-containing samples in the initial growth regime. Such an "induction/coalescence period" at the start of the CdS CBD has been observed before.[19–21] As the duration of this stage is strongly dependent on the chemical and morphological properties of the substrate,[22] it is most likely impacted by the presence of Rb at the treated absorber surface, e.g., by Cd-Rb ion exchange,[19] explaining the observed differences. After the initial "induction/coalescence period;" beginning with the 3 min

samples, the CdS leads more strongly attenuates the absorber-related signals of the RbF PDT sample than of the untreated absorber, consistent with Raman/SEM results[19] which indicate superior coverage.[1,23] A combined Raman/SEM study on similar samples indicates the latter.[19] After 15 min CBD no CIGSe related peak is visible on the RbF PDT sample (Figures S6 and S7, Supporting Information), which makes the determination of a distinct CdS layer thickness impossible, and also indicates a fully closed, compact CdS layer with thickness exceeding 3–4 × IMFP. The CdS thickness on the 2 min RISe/CIGSe sample, in contrast, is still smaller than the one on the untreated CIGSe after 3 min, indicating a longer "induction/coalescence period", which might indeed scale with the amount of Rb present at the sample surface.

To monitor the behavior of the Rb upon CdS deposition, the [Rb]/([Cu]+[In]+[Ga]+[Se]) ratio is calculated and displayed in Figure 3b, indicating no significant Rb increase or decrease with CdS deposition time (note that, due to the very low Rb content on the RbF PDT CIGSe sample, the Rb peak cannot be detected anymore in samples submitted to CBD treatments longer than 30 s). This lack of a trend in Rb content indicates that the Rb does not seem to diffuse into the buffer layer as Na is known to do.[24]

To investigate the impact of the CdS deposition on the observed RISe and the In-Se species formed upon RISe deposition, the [In_b]/[Rb] and [Se_b]/[Rb] as well as the [In_c]/[Se_c] ratios are displayed in Figure 3c,d. While the [In_c]/[Se_c] and [In_b]/[Rb] ratios show no significant changes when the CdS layer is deposited, indicating the chemical RISe/CIGSe structure to be unaffected by the CBD process of CdS, this is different in the case of the [Se_b]/[Rb], which shows a pronounced increase with CBD time. This could indicate a pronounced Se enrichment in the RISe phase during CdS layer growth, which is rather improbable, as no Rb-In-Se phase with a 1:1:4 stoichiometry is known. It could also indicate that the used fit model is insufficient and that an additional Se species might be formed upon CdS deposition. A possible candidate would be Cd-Se bonds, which have been shown to form at CdS/CIGSe interfaces.[25]

To investigate this, the Se 3d peak was fitted with a new model, allowing for an additional species (Se_d) and fixing the Se_b species, which accounts for the RISe phase, to the expected [Se_b]/[Rb] = 2 ratio based on the amount of Rb on the respective sample; the result is displayed in **Figure 4a**. The additional species, Se_d, compensates for the CdS CBD-induced shape changes of the peak. The position of that peak at ≈53.8 eV BE is very close to the RISe related Se_b species. However, the position is also in the energetic range where the Se 3d line of Cd—Se bonds is expected.[26–28] To further investigate the hypothesis of Cd-Se bond formation, the Cd 4d peak of the 3 min CBD CdS/ 2 min RISe/CIGSe sample was investigated, as on this sample the largest amount of Cd—Se bonds is expected according to the Se 3d fit. As the Cd 4d peak is at very low BE (≈11 eV) and therefore might be strongly impacted by hybridization, no fitting procedure is applied, but it is instead compared to the respective peak of the 3 min CdS/CIGSe sample on which no additional Se species was observed. Both peaks were normalized and plotted overlaying each other as displayed in Figure 4b. To further visualize the difference between the two spectra, a difference spectrum is added to the figure with a magnification factor of 10. This difference spectrum indicates an additional species is present for the 3 min CBD CdS/2 min RISe/CIGSe sample at higher BE (Cd $4d_{5/2}$ at

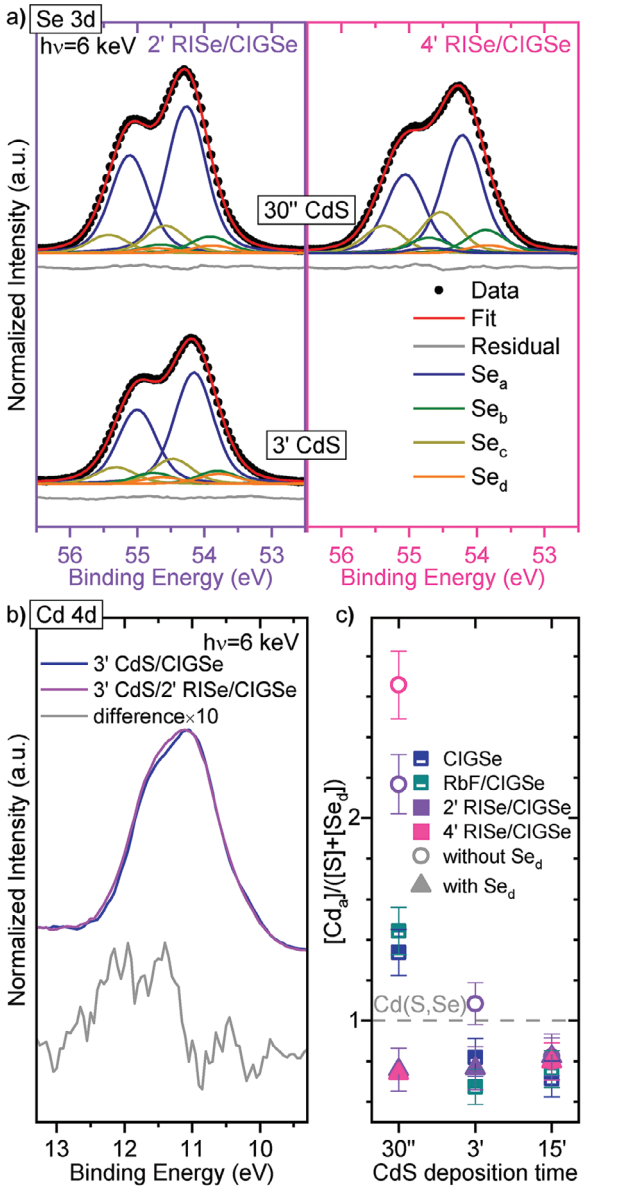

Figure 4. a) Se 3d spectra of the 30 s and 3 min CBD CdS on 2 min and 4 min RISe/CIGSe samples. Data are shown with a linear background subtracted. Respective fits are displayed along the data as are respective residuals. In the displayed fit model, the Se_b peak was restricted to a 2:1 ratio to the amount of Rb on the respective samples obtained from the spectra displayed in Figure S6 (Supporting Information). b) Cd 4d spectra of 3 min CBD CdS layers on CIGSe and 2 min RISe/CIGSe samples. Peaks are normalized and the difference between them is displayed with an offset and magnified by a factor of 10 as a gray line. c) Cation/anion ratio as [Cd_a]/([S]+[Se_d]) ratio, with and without the inclusion of [Se_d] on the anion side. The dashed line marks a 1:1 cation/anion ratio as expected for CdS and CdSe.

11.4 ± 0.2 eV) compared to the main peak (Cd $4d_{5/2}$ at 11.0 ± 0.1 eV); a position that agrees well with previous observations on CdSe contributions,[29] corroborating the suggestion of Cd-Se bond formation on the RISe treated samples. We cannot exclude that Cd—Se bond formation happens – to a lesser extent than on the RISe/CIGSe sample – for the CdS/CIGSe and the CdS/RbF

PDT CIGSe samples, as it has been reported for similar heterointerfaces in literature.[29,30] The Cd-Se formation and the duration of the "induction/coalescence period" of the CBD process (characterized primarily by $Cd(OH)_2$ adsorption on the CIGSe[21]) both appear to be enhanced by the presence of Rb.

To investigate how the buffer stoichiometry develops with deposition time and how it relates to the discussed formation of the Cd-Se bonds, the $[Cd_a]/[S]$ and $[Cd_a]/([S]+[Se_d])$ ratios were calculated based on the displayed fits of the Cd 4s, S 2s, and Se 3d peaks (Figures S6–S8, Supporting Information) and are displayed in Figure 4c. In the early stages of the CBD process there seems to be a significant S deficiency in all cases when considering the $[Cd_a]/[S]$ ratio (Cd_a is the main species; the secondary species Cd_b seen at higher BE is attributed to oxidized Cd[31]) The S-deficiency is, however, more pronounced in samples containing more Rb. If the Se_d species, attributed above to Cd—Se bonding, is included along with S (i.e., calculating $[Cd_a]/([S]+[Se_d])$), the anion deficiency vanishes and the cation to anion ratio in the buffer layer is constant throughout the deposition process on the samples displaying a Se_d species. This again is a clear indication for a pronounced Cd—Se bond formation in the early stages of the CBD. The S deficiency also occurs for the CdS layer CBD grown on untreated CIGSe and on RbF PDT CIGSe absorbers, possibly indicating that Cd—Se bonds may also be formed to a lesser extent on these absorbers, with the related additional Se species being below our detection limit. Making a more precise statement on the Cd–Se-type species, however, is difficult. Thomas Lepetit observed the formation of CdSe clusters in the early stages of CdS CBD on KF PDT CIGSe absorbers[30] but not on a KF free reference sample. Assuming the alkali element as the driving force for this formation and similar effects of K and Rb (or Na), the Cd—Se bonds could therefore relate to CdSe. However, also the presence of Cd-In-(Se,S,O,OH) compounds formed at the CdS/CIGSe interface, especially on alkali treated samples, has been discussed.[19,25,30] Although our investigation shows no indication of In being involved in an additional phase, parts of the detected Cd-Se bonds might still relate to such a phase with the In contribution being below our detection limit.

3. Conclusion

The chemical interface structures of (CdS/)RISe/CIGSe thin-film solar cell stacks have been studied and compared to that of (CdS/)CIGSe and (CdS/) RbF PDT CIGSe samples. While only a small amount of Rb and no indication for RISe formation can be found for the RbF PDT CIGSe absorber (presumably attributed to the high *CGI* of 0.95 and the relatively high IMFP of HAXPES compared to conventional XPS), there are clear indications of RISe formation for the RISe/CIGSe samples. However, the deposited cover layer is Rb-deficient compared to a stoichiometric $RbInSe_2$ phase, presumably due to Rb diffusion into the absorber. This Rb-deficient cover layer is described as a combination of stoichiometric $RbInSe_2$ and an additional In-Se phase.

When depositing a CBD CdS layer on the studied samples, a clear impact of the presence of (a) Rb (containing species) becomes apparent: in the early stages of the deposition no significant coverage of the absorber can be observed on the Rb (species) containing samples, with the duration of this "induction/coalescence period" of the CBD process seemingly scaling with the amount of Rb (species) on the sample. In the early stages of the CBD, formation of Cd—Se bonds is observed in particular on the RISe/CIGSe samples.

Linking our findings to the corresponding solar cell parameters published in ref. [9], the increasing V_{OC} with increasing RISe deposition time might be related to defect passivation by the RISe, the additional In-Se phase, or the Rb-diffusion into the bulk of the CIGSe, while the decreasing *FF* for solar cells with 3 min or longer RISe deposition, might be related to an increasing series resistance and/or the formation of a current extraction barrier due to the thicker cover layer. These competing effects lead to optimal device performance when RISe deposition is in the 2–4 min range.

These findings may contribute to understand the (beneficial) effect of the presence of Rb (species) at the buffer/absorber interface on the performance of respective solar cell devices.

4. Experimental Section

Sample Preparation and Handling: The samples were prepared at PVcomB using a high temperature (max. 530 °C) multistage process on Mo-coated soda-lime glass. The nominal [Cu]/([Ga]+[In]) (*CGI*) element ratio was 0.95. While one CIGSe absorber was kept free of Rb for comparison, another absorber underwent an RbF PDT consisting of the co-evaporation of RbF and Se for 10 min at a substrate temperature of 280 °C and a subsequent annealing step at the same temperature for 5 min without additional evaporation of RbF or Se. On the other absorbers, RISe layers with nominal thicknesses between 5 nm (1 min RISe evaporation) and 30 nm (6 min RISe evaporation) were deposited at a substrate temperature of 530 °C using the same procedure as described in ref. [11], leading to a nominal deposition rate of 5 nm min^{-1}. Note that the RbF PDT as well as RISe deposition were performed directly after finishing the CIGS preparation, without breaking the vacuum. A more detailed description of the absorber synthesis can be found in refs [9,18]. In addition, RISe was co-evaporated (thickness significantly larger than the detection depth) on Mo-coated soda-lime glass as reference. Details of the production and properties of this sample can be found in ref. [11]. To investigate the impact of the RbF PDT and the RISe deposition on the CdS buffer layer properties and buffer/absorber interface structure, CdS layers were deposited via chemical bath deposition (CBD) on the RISe/CIGSe samples as well as on the RbF PDT and the (control) untreated absorber. The time of the CBD was varied (30 s, 3 min, 15 min, with the latter being the standard deposition time for high-performing solar cells) to produce a buffer thickness series. Details of the buffer layer deposition can be found in ref. [18] 15 min CdS/RISe/CIGSe samples with 2 and 4 min RISe layers lead to the best-performing devices.[9] After fabrication, the samples were briefly exposed to air and stored in N_2 atmosphere, before being etched in aqueous NH_4OH solution for 3 min at room temperature to remove surface contaminants, subsequently rinsed in H_2O, double bagged in inert nitrogen atmosphere, and shipped to the SPring-8 synchrotron in Japan for HAXPES measurements (6 keV). For these measurements it was inevitable to expose the samples (again) to air for ≈2 h during mounting and introduction into the measurement system.

Synchrotron-Based Photoelectron Spectroscopy: HAXPES experiments were conducted at beamline BL15XU[32] of the SPring-8 storage ring. The base pressure of the HAXPES setup was $<10^{-8}$ mbar. It was equipped with a Scienta R4000 electron energy analyzer in a near-normal emission angle geometry. X-rays are horizontally polarized, with the direction of polarization normal to the analyzer entrance slit. Spectra were recorded using calibrated photon energies of 5.95 keV (referred to as 6 keV in this work) monochromatized with a Si(111) double-crystal monochromator and a high-resolution Si(333) channel-cut monochromator. This results in an information depth (defined as three times inelastic mean free path – IMFP – accounting for ≈95% of the measured signal) of ≈25 nm which was

sufficient to monitor most of the interfaces of the samples and layers described above. A pass energy of 200 eV was used for all measurements, resulting in a combined analyzer plus beamline resolution of ≈0.25 eV. The binding energy (BE) was calibrated by referencing the Au $4f_{7/2}$ peak of a grounded clean Au foil to a binding energy of 84.00 eV.

Curve Fit Analysis: Core levels were fitted using linear backgrounds and Voigt profiles, keeping – if more than one species was present – the interspecies energy separation of one core level constant for all excitation energies and keeping the shape of the Voigt identical for identical core levels. For core-levels with a splitting due to spin orbit coupling (i.e., all core levels with $l > 0$), two Voigt profiles with a fixed splitting and a fixed ratio according to $\frac{1+2(l+\frac{1}{2})}{1+2(l-\frac{1}{2})}$ were used.[33]

Stoichiometry Calculation: For calculating elemental ratios, shallow core levels (Cd 4s, Rb 3d, Cu 3p, Na 2s, Se 3d, Ga 3d, In 4 d) were only corrected by photoionization cross-section,[34,35] as the kinetic energy of the respective photoelectrons was very similar and thus any impact of different IMFP and a different analyzer transmission was negligible. The S 2s core level was additionally corrected by analyzer transmission function and IMFP,[16] as its binding energy differs by ≈200 eV from that of the shallow core levels.

Cover Layer Thickness Calculation: Buffer layer thicknesses "*d*" were calculated using the Lambert-Beer-law: $d = IMFP * \ln(\frac{I_0}{I_d})$ with $\frac{I_0}{I_d}$ being the ratio of absorber-related photoemission intensities prior and after buffer layer deposition. For the two calculated buffer layers, IMFP values of 8.6 nm (RISe) and 9.8 nm (CdS) were used.[16]

Supporting Information

Supporting Information is available from the Wiley Online Library or from the author.

Acknowledgements

J.B. acknowledges support from the Graduate School Materials for Solar Energy Conversion (MatSEC) as part of Dahlem Research School. The HAXPES measurements at SPring-8 were performed under an approval of NIMS Synchrotron X-ray Station (Proposal No. 2019A4910) and was supported by NIMS microstructural characterization platform as a program of "Nanotechnology Platform" (project No. 12024046) of the Ministry of Education, Culture, Sports, Science and Technology (MEXT), Japan.

Open access funding enabled and organized by Projekt DEAL.

Conflict of Interest

The authors declare no conflict of interest.

Data Availability Statement

The data that support the findings of this study are available from the corresponding author upon reasonable request.

Keywords

chalcopyrite thin-film solar cells, HAXPES, RbF-PDT, $RbInSe_2$

Received: February 29, 2024
Revised: March 31, 2024
Published online: May 6, 2024

[1] A. Chirilă, P. Reinhard, F. Pianezzi, P. Bloesch, A. R. Uhl, C. Fella, L. Kranz, D. Keller, C. Gretener, H. Hagendorfer, D. Jaeger, R. Erni, S. Nishiwaki, S. Buecheler, A. N. Tiwari, *Nat. Mater.* **2013**, *12*, 1107.
[2] P. Jackson, D. Hariskos, R. Wuerz, O. Kiowski, A. Bauer, T. M. Friedlmeier, M. Powalla, *Phys. Status Solidi RRL – Rapid Res. Lett.* **2015**, *9*, 28.
[3] M. Nakamura, K. Yamaguchi, Y. Kimoto, Y. Yasaki, T. Kato, H. Sugimoto, *IEEE J. Photovolt.* **2019**, *9*, 1863.
[4] M. Malitckaya, H.-P. Komsa, V. Havu, M. J. Puska, *J. Phys. Chem. C* **2017**, *121*, 15516.
[5] E. Handick, P. Reinhard, R. G. Wilks, F. Pianezzi, T. Kunze, D. Kreikemeyer-Lorenzo, L. Weinhardt, M. Blum, W. Yang, M. Gorgoi, E. Ikenaga, D. Gerlach, S. Ueda, Y. Yamashita, T. Chikyow, C. Heske, S. Buecheler, A. N. Tiwari, M. Bär, *ACS Appl. Mater. Interfaces* **2017**, *9*, 3581.
[6] J. Bombsch, E. Avancini, R. Carron, E. Handick, R. Garcia-Diez, C. Hartmann, R. Félix, S. Ueda, R. G. Wilks, M. Bär, *ACS Appl. Mater. Interfaces* **2020**, *12*, 34941.
[7] N. Taguchi, S. Tanaka, S. Ishizuka, *Appl. Phys. Lett.* **2018**, *113*, 113903.
[8] N. Maticiuc, T. Kodalle, J. Lauche, R. Wenisch, T. Bertram, C. A. Kaufmann, I. Lauermann, *Thin Solid Films* **2018**, *665*, 143.
[9] T. Kodalle, T. Bertram, R. Schlatmann, C. A. Kaufmann, *IEEE J. Photovolt.* **2019**, *9*, 1839.
[10] T. P. Weiss, S. Nishiwaki, B. Bissig, R. Carron, E. Avancini, J. Löckinger, S. Buecheler, A. N. Tiwari, *Adv. Mater. Interfaces* **2017**, *5*, 1701007.
[11] T. Kodalle, R. K. M. Raghupathy, T. Bertram, N. Maticiuc, H. A. Yetkin, R. Gunder, R. Schlatmann, T. D. Kühne, C. A. Kaufmann, H. Mirhosseini, *Phys. Status Solidi RRL – Rapid Res. Lett.* **2019**, *13*, 1800564.
[12] E. Avancini, R. Carron, T. P. Weiss, C. Andres, M. Bürki, C. Schreiner, R. Figi, Y. E. Romanyuk, S. Buecheler, A. N. Tiwari, *Chem. Mater.* **2017**, *29*, 9695.
[13] T. Kodalle, M. D. Heinemann, D. Greiner, H. A. Yetkin, M. Klupsch, C. Li, P. A. Aken, I. Lauermann, R. Schlatmann, C. A. Kaufmann, *Sol. RRL* **2018**, *2*, 1800156.
[14] J. Bombsch, E. Avancini, R. Carron, E. Handick, R. Garcia-Diez, C. Hartmann, R. Félix, D. Abou-Ras, S. Ueda, R. G. Wilks, M. Bär, *Adv. Energy Sustain. Res.* **2021**, *2*, 2100101.
[15] M. Guc, T. Kodalle, R. Kormath Madam Raghupathy, H. Mirhosseini, T. D. Kühne, I. Becerril-Romero, A. Pérez-Rodríguez, C. A. Kaufmann, V. Izquierdo-Roca, *J. Phys. Chem. C* **2020**, *124*, 1285.
[16] S. Tanuma, C. J. Powell, D. R. Penn, *Surf. Interface Anal.* **1993**, *20*, 77.
[17] S. Tanuma, C. J. Powell, D. R. Penn, *Surf. Interface Anal.* **1994**, *21*, 165.
[18] T. Kodalle, Unraveling the Structural and Optoelectronic Effects of Rb on Chalcopyrite Solar Cells. PhD Thesis **2020**.
[19] T. Kodalle, L. Choubrac, L. Arzel, R. Schlatmann, N. Barreau, C. A. Kaufmann, *Sol. Energy Mater. Sol. Cells* **2019**, *200*, 109997.
[20] L. Choubrac, G. Brammertz, N. Barreau, L. Arzel, S. Harel, M. Meuris, B. Vermang, *Phys. Status Solidi A* **2018**, *215*, 1800043.
[21] P. O'Brien, J. McAleese, *J. Mater. Chem.* **1998**, *8*, 2309.
[22] D. Lincot, J. Vedel, In Tenth E.C. Photovoltaic Solar Energy Conference, (Eds: A. Luque, G. Sala, W. Palz, G. Santos, P. Helm), Springer Netherlands, Dordrecht **1991**, pp 931.
[23] T. M. Friedlmeier, P. Jackson, D. Kreikemeyer-Lorenzo, D. Hauschild, O. Kiowski, D. Hariskos, L. Weinhardt, C. Heske, M. Powalla, In 2016 IEEE 43rd Photovoltaic Specialists Conf. (PVSC), Portland, OR, USA, June **2016**, pp 0457.
[24] H. A. Yetkin, T. Kodalle, T. Bertram, A. Villanueva-Tovar, R. Klenk, B. Szyszka, R. Schlatmann, C. A. Kaufmann, In 2020 47th IEEE Photovoltaic Specialists Conf. (PVSC), Calgary, AB, Canada **2020**, pp 1192.
[25] P. Yang, R. G. Wilks, W. Yang, M. Bär, *ACS Appl. Mater. Interfaces* **2020**, *12*, 6688.
[26] R. Islam, D. R. Rao, *J. Electron Spectrosc. Relat. Phenom.* **1996**, *81*, 69.
[27] H. Rupp, U. Weser, *Bioinorg. Chem.* **1975**, *5*, 21.

[28] M. Polak, *J. Electron Spectrosc. Relat. Phenom.* **1982**, *28*, 171.
[29] L. Ley, R. A. Pollak, F. R. McFeely, S. P. Kowalczyk, D. A. Shirley, *Phys. Rev. B* **1974**, *9*, 600.
[30] T. Lepetit, Influence of KF Post Deposition Treatment on the Polycrystalline Cu(In,Ga)Se2/CdS Hetero-Junction Formation for Photovoltaic Application, *Doctoral Thesis*, Université de Nantes, Nantes, **2015**.
[31] D. Kreikemeyer-Lorenzo, D. Hauschild, P. Jackson, T. M. Friedlmeier, D. Hariskos, M. Blum, W. Yang, F. Reinert, M. Powalla, C. Heske, L. Weinhardt, *ACS Appl. Mater. Interface* **2018**, *10*, 37602.
[32] S. Ueda, Y. Katsuya, M. Tanaka, H. Yoshikawa, Y. Yamashita, S. Ishimaru, Y. Matsushita, K. Kobayashi, *AIP Conf. Proc.* **2010**, *1234*, 403.
[33] F. de Groot, A. Kotani, *Core Level Spectroscopy of Solids*, 1st ed., CRC Press, Boca Raton, FL **2008**.
[34] M. B. Trzhaskovskaya, V. I. Nefedov, V. G. Yarzhemsky, *At. Data Nucl. Data Tables* **2001**, *77*, 97.
[35] M. B. Trzhaskovskaya, V. K. Nikulin, V. I. Nefedov, V. G. Yarzhemsky, *At. Data Nucl. Data Tables* **2006**, *92*, 245.